Letter

# Mott correlations in ABC graphene trilayer aligned with hBN

M. J. Calderón [1,*] A. Camjayi,[2] and E. Bascones [1,†]

[1]*Instituto de Ciencia de Materiales de Madrid (ICMM). Consejo Superior de Investigaciones Científicas (CSIC), Sor Juana Inés de la Cruz 3, 28049 Madrid, Spain*

[2]*Ciclo Básico Común, Universidad de Buenos Aires and IFIBA, Conicet, Pabellón 1, Ciudad Universitaria, 1428 CABA, Argentina*

(Received 25 April 2022; accepted 5 August 2022; published 25 August 2022)

ABC trilayer graphene aligned with hexagonal boron nitride (ABC/hBN) and other moiré systems have shown insulating phases at integer fillings of the moiré lattice. The role of Mott physics in these insulating states has been questioned by observations of correlated states in a nonaligned ABC trilayer, but recent photocurrent experiments in aligned samples are consistent with the existence of a Mott insulating state at half filling. Using dynamical mean-field theory we address the effect of Mott correlations in ABC/hBN. We show that, at experimentally relevant interaction values, the electronic states are strongly affected by a significant spectral weight transfer not present without alignment to hBN. This effect, which emerges at interactions considerably smaller than $U_{\mathrm{Mott}}$ (at which the Mott metal-insulator transition takes place) and does not require symmetry breaking, also impacts the electronic properties at temperatures above the ordering transitions producing anomalous temperature and doping dependencies. Close to the Mott transition, the intramoiré unit cell interactions promote an antiferromagnetic state, probably breaking the $C_3$ symmetry, that would compete with the ferromagnetic exchange interactions to determine the ground state.

DOI: 10.1103/PhysRevB.106.L081123

Since the discovery of insulating phases and superconductivity in magic angle twisted bilayer graphene (MATBG) [1,2], moiré structures with narrow bands have become new platforms to explore electronic correlations [3–9]. The phase diagrams of several moiré systems resemble those of correlated materials such as high-$T_c$ superconductors or heavy fermions [10–15], where local correlations produce a plethora of unconventional behaviors, including Mott insulating states. A key issue is whether local correlations are also of relevance in moiré systems or their states can be well explained in terms of standard band instabilities. ABC trilayer graphene aligned with hexagonal boron nitride (ABC/hBN), the first moiré system to show insulating states after MATBG [3], is playing a prominent role in this Letter. The moiré potential originates in the alignment between graphene and hBN, both with honeycomb structures but slightly different lattice constants [Figs. 1(a) and 1(b)]. The effect of the moiré confinement on the correlated states and, as discussed below, the role of Mott correlations in aligned samples may be addressed by comparing experimental signatures in nonaligned and aligned samples.

ABC trilayer graphene features bands with flat sections close to the charge neutrality point (CNP), owing to their cubic dispersion in the absence of trigonal warping [16–18]. A perpendicular electric field induces a potential drop $\delta_V$ between the top and bottom graphene layers, opening a gap at the CNP and making the bands flatter. If the ABC trilayer is aligned to hBN, the superlattice potential gaps the bands at the boundaries of the moiré mini-Brillouin zone giving rise to narrow bands, isolated with a perpendicular electric field [3]. The bandwidth $W$, the filling $n$, and the topological properties of these bands can be further tuned by gates, with the valence band narrower than the conduction band. Depending on the $\delta_V$ orientation with respect to hBN, the valence band can be topologically trivial (Chern number $\nu = 0$) or not ($\nu = \pm 3$) [19–21]. Correlated insulating states have been observed in ABC/hBN for both signs of $\delta_V$ and one or two holes added to the valence band [3,22,23]. Due to the valley and spin degeneracy, up to four holes can be accommodated and half filling occurs at $n = -2$. Evidence of correlations such as ferromagnetism (FM) has been observed at some metallic fillings [23,24].

Spin and/or valley polarized metallic phases and superconductivity have been recently observed in nonaligned ABC graphene trilayers under an electric field for electronic densities similar to those of the correlated states in ABC/hBN [23,25]. In a nonaligned ABC trilayer there is no moiré confining potential, and at the experimental densities the electronic doping per unit cell is very far away from integer fillings, ruling out any role of Mott physics at such low densities. The polarized phases were ascribed to the large density of states (DOS) enhanced by the electric field, with FM originating in a Stoner instability [23,25]. In aligned samples, the moiré potential enlarges the unit cell and at certain values of the experimental densities the electronic doping per moiré unit cell is an integer allowing Mott physics to play a role in the observed features. Compressibility measurements in aligned and nonaligned trilayers exhibit strong

*mariaj.calderon@csic.es
†leni.bascones@csic.es

 

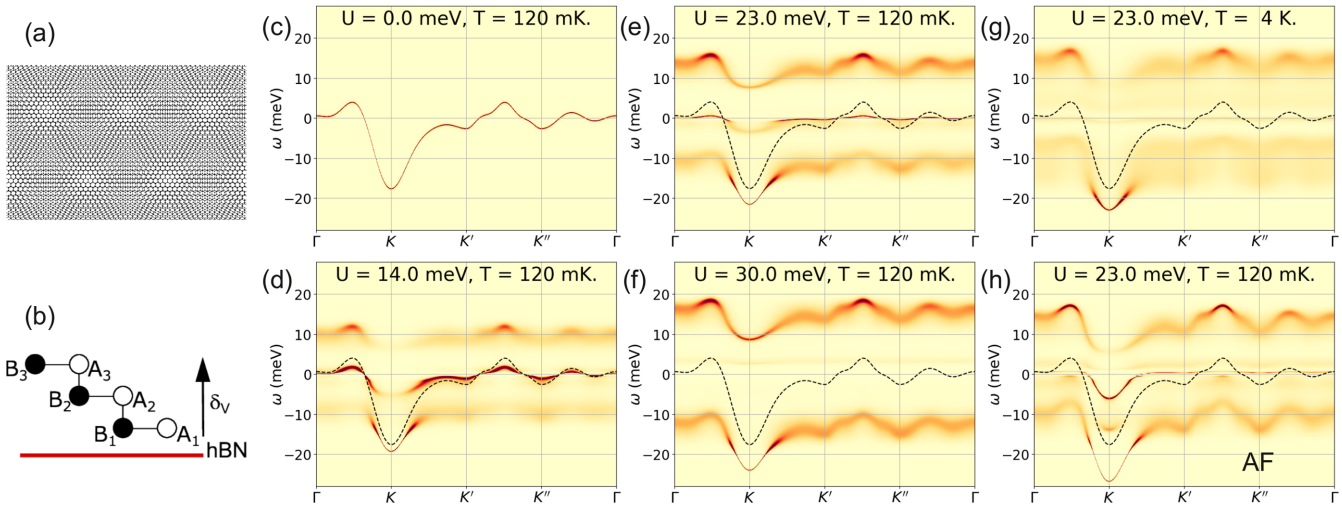


FIG. 1. (a) Moiré pattern due to a lattice mismatch between two honeycomb layers (not to scale). The moiré length in ABC/hBN is $a_M \approx 15$ nm. (b) Sketch of ABC/hBN. $A_i$ and $B_i$ are the carbon sublattices in each graphene layer. Only one layer is aligned to hBN. (c)–(h) Spectral weight on the valence band of a given valley for $\delta_V = 30$ meV at half filling $n = -2$. Each curve is centered at its corresponding chemical potential $\mu$. The dashed line in (d)–(h) is a guide to the eye for the noninteracting band in (c). (c)–(f) correspond to $U = 0$, 14, 23, and 30 meV at $T = 120$ mK, imposing an SU(4) symmetric solution. As $U$ increases, the quasiparticle band gets renormalized, the Fermi velocity is reduced, and the electronic states away from $\mu$ have finite probability to decay, giving a blurred aspect to the band, and part of the spectral weight is transferred to the incoherent Hubbard bands (around $\pm U/2$). The quasiparticle band disappears at the Mott transition at $U_{\text{Mott}} \sim 28$ meV. (g) Bands with $U = 23$ meV at $T = 4$ K. (h) Bands in a spin-AFM broken symmetry state for $U = 23$ meV at $T = 120$ mK.

similarities [23]. Important differences induced by the alignment include incompressible states at 1 and 2 holes/electrons per moiré unit cell, not allowed without the moiré, and a lack of symmetry with respect to the $\delta_V$ sign. Relying on the similarities, Ref. [23] concluded that the correlated states in ABC/hBN, including the insulating ones, originate in an itinerant FM Stoner instability, with the moiré potential and band isolation being just a perturbation and Mott correlations playing essentially no role. However, a recent work has reported a broad absorption peak at ∼18 meV in the photocurrent spectrum of ABC/hBN at $n = -2$, absent at CNP, which is consistent with a direct optical excitation across a Mott gap but not expected for full ferromagnetic spin or valley polarization [26]. The specific features able to clarify the role of Mott physics [27–29] in ABC/hBN have yet to be addressed theoretically.

Here, we use dynamical mean-field theory (DMFT) to study the effect of the local correlations on the isolated topologically trivial valence band in ABC/hBN with the focus on the reorganization of the electronic spectral weight. This reorganization eventually leads to a Mott transition at integer fillings and high interactions but is already prominent in the metallic state. The strong band narrowing and the incoherent spectral weight produced by the local correlations results in unconventional doping-dependent electronic properties, as detected here in the density of states. We have found that close to the Mott transition the intramoiré unit-cell interactions promote an antiferromagnetic (AFM) ordering in ABC/hBN, probably breaking $C_3$ symmetry, that would compete with the FM intersite exchange interactions to determine the ground state. The reorganization of the spectral weight induced by Mott correlations does not require symmetry breaking and the incoherence is enhanced with increasing $T$. In order to discern purely Mott features from signals coming from ordered states in ABC/hBN, we propose to study the doping and $T$-dependent electronic properties above the ordering $T_{\text{AFM}}$.

We study the effect of correlations in ABC/hBN with density-density interactions incorporated in an effective intramoiré unit-cell interaction $U$, with a range of magnitudes expected to be relevant in experiments (see Supplemental Material [30]). In our approximation, the interactions are SU(4) symmetric, accounting for the spin and valley symmetry. The effect of the much smaller exchange terms is qualitatively addressed in the discussion. Except as otherwise stated, we give results for $\delta_V = 30$ meV. The noninteracting electronic band and the density of states (DOS) are plotted in Figs. 1(c) and 2(a).

*Nonordered state*. Many Mott insulators order at low $T$ but the Mott transition does not require any symmetry breaking. Hence, the Mott character of a transition is more easily identified in the nonordered state. Figures 1(c)–1(f) show the spectral weight $A(\mathbf{k}, \omega)$ for one of the valleys as a function of interaction $U$ at $n = -2$ and low temperature ($T = 120$ mK) in the nonordered state. The SU(4) symmetry solution has been imposed in the DMFT calculation. The energy of the states in the noninteracting band in Fig. 1(c) is well defined, and the band is sharp and thin, as the single-electron states are eigenstates of the Hamiltonian, i.e., they do not decay. At $U = 14$ meV $< W \sim 20$ meV, the effect of the electronic correlations on the band shape is already quite evident [Fig. 1(d)]. The single-electron states are no longer eigenstates of the interacting Hamiltonian and its lifetime is finite. Two features stand out: the appearance of two incoherent bands separated by $\sim U$ and a strongly renormalized band at the Fermi energy. The incoherent (Hubbard) bands are not well defined. The renormalized band around the Fermi level is better defined,

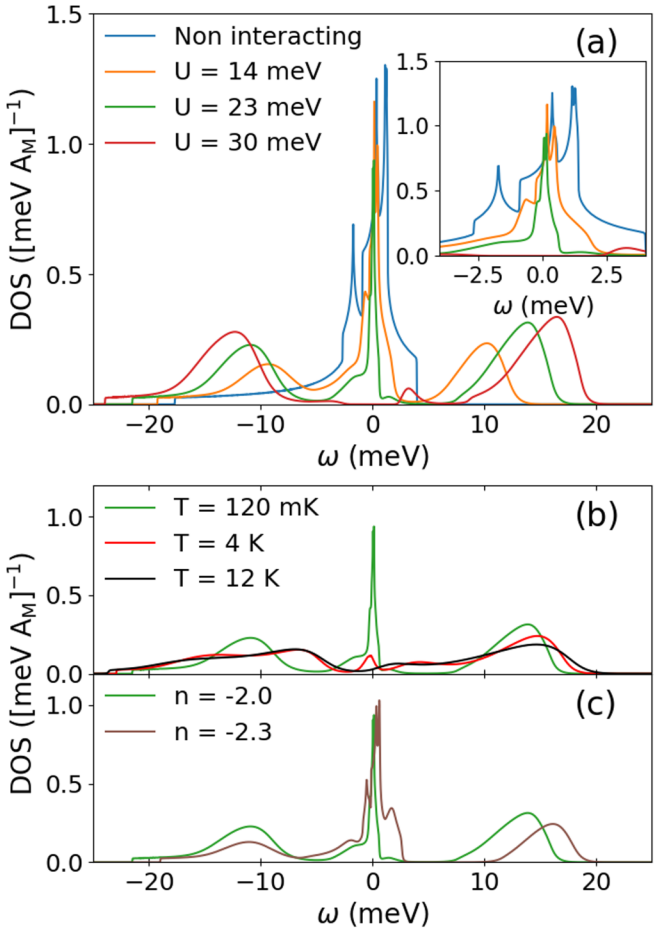


FIG. 2. Density of states (a) for different values of $U$ at $T = 120$ mK and half filling $n = -2$. Inset: Zoom at low frequencies; (b) for different $T$ at $U = 23$ meV and $n = -2$; (c) for different $n$ at $U = 23$ meV and $T = 120$ mK. Each curve is centered at its corresponding chemical potential.

its effective mass has been enhanced, and its width is finite but small. These are heavy quasiparticle states, a truly many-body superposition of single-particle states. The effect of the correlations is more evident at $U = 23$ meV [Fig. 1(e)]. The quasiparticle band around $\omega = 0$ has become very narrow and it has lost most of its spectral weight, while the Hubbard bands are well formed. At $U = 30$ meV, in the Mott insulator, there is no band crossing the chemical potential [Fig. 1(f)]. The quasiparticle band disappears at the Mott transition at $U_{\text{Mott}} \sim 28$ meV.

The strong reorganization of the spectral weight is manifest in the DOS which for $U < U_{\text{Mott}}$ shows the characteristic three-peak structure of correlated metals approaching the Mott transition [31,32] [Fig. 2(a)]. In accordance with the effect in the bands, the quasiparticle peak around the chemical potential narrows with increasing $U$, losing spectral weight which accumulates in the Hubbard bands at positive and negative energies. For $U = 0$, around 81% of the total spectral weight is within $-3$ and 4 meV from the chemical potential, but this percentage is reduced to 41% and 19% at $U = 14$ and 23 meV, respectively. At $U = 30$ meV, above $U_{\text{Mott}}$, the quasiparticle peak is absent. Almost all the spectral weight has been transferred to the Hubbard bands.

The incoherence grows with increasing $T$. This is already evident at a few degrees Kelvin. At 4 K, a $T$ much smaller than the noninteracting $W$, the quasiparticle band at $U = 23$ meV cannot be distinguished in Fig. 1(g). Concomitantly, the peak in the DOS at the chemical potential is suppressed [Fig. 2(b)]. Doping away from integer filling favors the metallic states and correlations induce changes in the DOS and a nonrigid band shift. In Fig. 2(c), the width of the quasiparticle peak in the DOS is larger at $n = -2.3$ than at $n = -2$, showing a closer resemblance, also in shape, to the noninteracting DOS in Fig. 2(a). At $U = 14$ meV, considerably far from the Mott transition, the enhancement of the incoherence at a few degrees Kelvin and the change of the quasiparticle peak width with doping are less pronounced but still visible [30].

*Ordered state*. We now allow for the breaking of spin and/or valley symmetry. At $n = -2$, we have found an AFM ordered state with broken SU(4) spin-valley symmetry. Due to the underlying symmetry of the interactions considered, in which the Hund's coupling $J_{\text{H}}$ or any other SU(4) symmetry breaking interaction terms are assumed to be zero, the spin-AFM and the AFM-valley ordering are degenerate and equally stable. Figure 3(a) shows the order parameter $\Delta n_{\text{AFM}}$ as a function of $U$. $\Delta n_{\text{AFM}}$, with a maximum possible value of 2, is defined as the intra-unit-cell difference in occupation between the two valleys $\Delta n_{\text{AFM}} = \sum_\sigma (n_{\zeta,\sigma} - n_{\bar{\zeta},\sigma})$ in the pure AFM-valley state or the two spins $\Delta n_{\text{AFM}} = \sum_\zeta (n_{\zeta,\sigma} - n_{\zeta,\bar{\sigma}})$ in the pure spin AFM but other combinations of spin $\sigma$ and valley $\zeta$ AFM are possible. The ordering at $n = -2$ emerges at $U \sim 0.7 U_{\text{Mott}}$ and remains in the Mott insulator up to at least 31 meV. We found difficulties in converging the AFM state beyond this interaction and we cannot confirm whether this state is stable at larger $U$. The AFM order persists up to $T \sim 3$–4 K [inset in Fig. 3(a)], compatible with the energy gain due to the AFM $\sim 0.25$ meV [30]. In spite of the small energy gain, much smaller than the effective interaction $U$, the AFM ordering induces changes in the spectral weight in a large energy window [compare Figs. 1(e) and 1(h)]. Above $U \sim 20.5$ meV the kinetic energy decreases in the AFM state while the potential energy increases. This suggests that the AFM is stabilized by superexchange processes, in accordance with the AFM being stable only close to the Mott insulating state and consistent with the doping dependence. We have found that the AFM state is weakly metallic below $U_{\text{Mott}}$, but it is not a Fermi liquid very close to the transition [30]. Doping away from $n = -2$ quickly suppresses the ordering [see Figs. 3(b) and 3(c)], with AFM surviving to changes in $n$ of only $\sim \pm 0.1$ holes per moiré unit cell.

We have found a similar AFM state with $\delta_V = 20$ meV and $\delta_V = 50$ meV (not shown). Within the DMFT calculations performed here, we cannot identify the AFM ordering pattern. Nevertheless, considering the states that can be stabilized within our calculations, we believe that the AFM ordering found has the $C_3$ symmetry breaking pattern found in Ref. [33] [see the inset in Fig. 3(c)], by performing variational Monte Carlo calculations (VMC) for $\delta_V = 20$ meV and $n = -2$. Within the range of parameters studied in Ref. [33], $J_{\text{H}} \neq 0$ seemed necessary to stabilize the AFM state, breaking the SU(4) symmetry of the interactions. In their calculations the ground state was a spin-AFM, while an AFM-valley ground state was not stabilized. The lack of order at $J_{\text{H}} = 0$ in

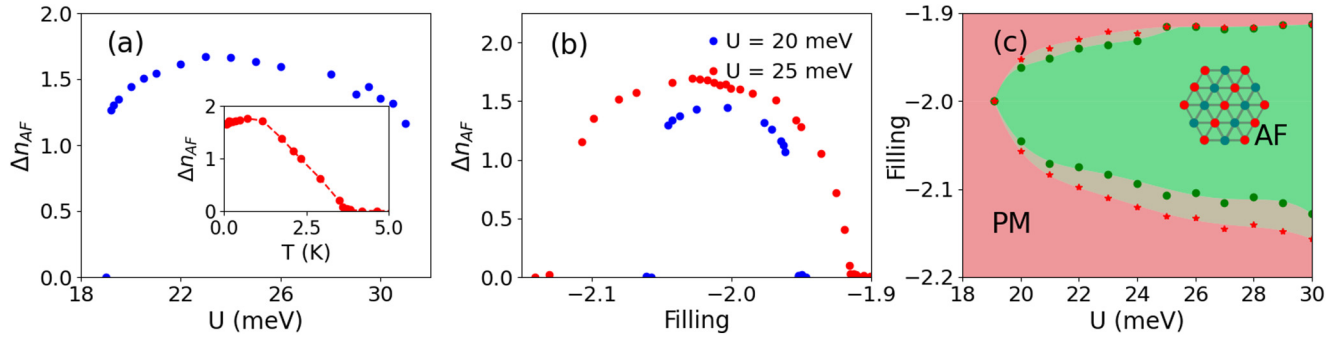


FIG. 3. (a) Order parameter $\Delta n_{\mathrm{AFM}}$ in the AFM state as a function of $U$ at $n = -2$ and $T = 120$ mK. The inset: $\Delta n_{\mathrm{AFM}}$ vs $T$ for $U = 23$ meV and $n = -2$. (b) $\Delta n_{\mathrm{AFM}}$ as a function of filling around $n = -2$ for $U = 20$ meV and $U = 25$ meV. (c) Phase diagram as a function of $n$ and $U$. In the AFM green region, $\Delta n_{\mathrm{AFM}} \neq 0$, and in the nonordered (PM) red one, $\Delta n_{\mathrm{AFM}} = 0$. The shaded area between the two regions is inhomogeneous [30]. Inset: $C_3$ symmetry breaking AFM ordering proposed in the main text. Red and green dots account for two opposite degrees of freedom, such as two opposite spins or valleys.

Ref. [33] is most probably due to the value of the interaction $U = 0.93\tilde{W}$ studied in that work, with $\tilde{W}$ the $\delta_V = 20$ meV bandwidth. This $U$ is considerably smaller than $\tilde{U}_{\mathrm{Mott}} \sim 1.5\tilde{W}$ for $\delta_V = 20$ meV and $J_{\mathrm{H}} = 0$ according to our calculations. In agreement with Ref. [33], we have not found AFM at $n = -2$ for $U = 0.93\tilde{W}$ and $\delta_V = 20$ meV.

*Discussion.* The spectral weight reorganization discussed here is one of the main signatures of Mott physics. The details of the isolated noninteracting band would not change qualitatively the picture discussed here, but they could have some influence in $U_{\mathrm{Mott}}$ and on the magnetic orderings. Importantly, this spectral weight transfer is already significant at values of $U$ below the Mott transition. In such a case, the system behaves as a correlated metal at $T$ above any ordering transition affecting the electronic properties. The reorganization of spectral weight alters the density of states with consequences in the ordering tendencies and in experimental properties such as transport or optical measurements. A detailed theoretical analysis of these effects is beyond the scope of this Letter and is left for future work. Nevertheless it includes optical transitions between the Hubbard bands, changes in the spectrum at energy scales much larger than the ordering temperatures, and non-Fermi-liquid behavior in a certain range of temperatures [29]. If Mott correlations are relevant in ABC/hBN, they will also show up in the nonordered state, insulating or metallic, at integer fillings of the moiré unit cell. In ABC graphene trilayers, Mott correlations are only expected in the presence of the moiré confining potential, with the flat valence band isolated. The unconventional behavior in the nonordered state should not be present in the nonaligned trilayer. Therefore comparing aligned and nonaligned samples facilitates identifying the effects discussed here. This would allow us to distinguish the relevance of Mott correlations from the proposal, arising from the observed similarities in the metallic states of aligned and nonaligned samples, that the insulating states at integer fillings in ABC/hBN are a consequence of a Stoner instability [23].

Our picture is supported by the emergence of an optically active transition in the insulating state at $n = -2$ in recent photocurrent experiments in aligned samples [26]. This is not expected in a FM fully polarized state due to optical selection rules but is consistent with a transition between Hubbard bands. Whether the system is in an ordered or nonordered state in these measurements is not yet clear but could be studied in future experiments as a function of temperature. The absorption peak between the Hubbard bands should persist at metallic dopings close to half filling though with a reduced intensity. Photocurrent experiments in the metallic state are challenging but the optical transition could impact other experiments.

In the calculations we neglected the on-site and intersite exchange terms. These terms were estimated to be much smaller than the density-density interactions [19] and therefore they are not expected to alter significantly the nonordered state. On the other hand, they are comparable to the energy gain due to the AFM ordering found and could modify the predictions in the ordered state. On general grounds, $J_{\mathrm{H}} \neq 0$ breaks SU(4) symmetry such that spin and valley ordering would be nondegenerate. Whether spin or valley order is promoted depends on the sign of $J_{\mathrm{H}}$. Reference [19] estimated $J_{\mathrm{H}} \approx +0.1$ meV but its value is currently under discussion [23].

The small overlap between the wave functions at neighboring unit cells produces an intersite exchange interaction $I_{\mathrm{H}} \approx 0.4$ meV [19]. $I_{\mathrm{H}}$ favors FM and would compete with the AFM ordering due to superexchange found in this work. VMC calculations for $\delta_V = 20$ meV [33] found FM order with $I_{\mathrm{H}} > 0.3$ meV. FM mediated by intersite exchange is therefore a plausible ground state even in proximity to the Mott transition or insulating state. The energy difference between the FM and AFM orderings is expected to be comparable to the energy scales of external perturbations such as magnetic fields or strains, opening the possibility to experimentally tune the transition between different magnetic states by external knobs, which would clarify the role of superexchange and intersite mechanisms. In summary, our work identifies the signatures that may guide future experiments to elucidate the role of Mott correlations in ABC/hBN.

M.J.C. and E.B. acknowledge funding from PGC2018-097018-B-I00 (MCIN/AEI/FEDER, EU). A.C. acknowledges support from UBACyT (Grant No. 20020170100284BA) and Agencia Nacional de Promoción de la Investigación, el Desarrollo Tecnológico y la Innovación (Grant No. PICT-2018-04536).

[1] Y. Cao, V. Fatemi, A. Demir, S. Fang, S. L. Tomarken, J. Y. Luo, J. D. Sanchez-Yamagishi, K. Watanabe, T. Taniguchi, E. Kaxiras, R. C. Ashoori, and P. Jarillo-Herrero, Correlated insulator behaviour at half-filling in magic-angle graphene superlattices, Nature (London) **556**, 80 (2018).

[2] Y. Cao, V. Fatemi, S. Fang, K. Watanabe, T. Taniguchi, E. Kaxiras, and P. Jarillo-Herrero, Unconventional superconductivity in magic-angle graphene superlattices, Nature (London) **556**, 43 (2018).

[3] G. Chen, L. Jiang, S. Wu, B. Lyu, H. Li, B. L. Chittari, K. Watanabe, T. Taniguchi, Z. Shi, J. Jung, Y. Zhang, and F. Wang, Evidence of a gate-tunable Mott insulator in a trilayer graphene moiré superlattice, Nat. Phys. **15**, 237 (2019).

[4] X. Liu, Z. Hao, E. Khalaf, J. Y. Lee, Y. Ronen, H. Yoo, D. Haei Najafabadi, K. Watanabe, T. Taniguchi, A. Vishwanath, and P. Kim, Tunable spin-polarized correlated states in twisted double bilayer graphene, Nature (London) **583**, 221 (2020).

[5] Z. Hao, A. Zimmerman, P. Ledwith, E. Khalaf, D. H. Najafabadi, K. Watanabe, T. Taniguchi, A. Vishwanath, and P. Kim, Simulation of Hubbard model physics in $WSe_2/WS_2$ moiré superlattices, Nature (London) **579**, 353 (2020).

[6] J. M. Park, Y. Cao, K. Watanabe, T. Taniguchi, and P. Jarillo-Herrero, Tunable strongly coupled superconductivity in magic-angle twisted trilayer graphene, Nature (London) **590**, 249 (2021).

[7] Z. Hao, A. Zimmerman, P. Ledwith, E. Khalaf, D. H. Najafabadi, K. Watanabe, T. Taniguchi, A. Vishwanath, and P. Kim, Electric field-tunable superconductivity in alternating twist magic-angle trilayer graphene, Science **371**, 1133 (2021).

[8] Y. Zhang, R. Polski, C. Lewandowski, A. Thomson, Y. Peng, Y. Choi, H. Kim, K. Watanabe, T. Taniguchi, J. Alicea, F. von Oppen, G. Refael, and S. Nadj-Perge, Ascendance of superconductivity in magic-angle graphene multilayers, arXiv:2112.09270.

[9] J. M. Park, Y. Cao, L.-Q. Xia, S. Sun, K. Watanabe, T. Taniguchi, and P. Jarillo-Herrero, Robust superconductivity in magic-angle multilayer graphene family, Nat. Mater. **21**, 877 (2022).

[10] B. Keimer, S. Kivelson, M. Norman, S. Uchida, and J. Zaanen, From quantum matter to high-temperature superconductivity in copper oxides, Nature (London) **518**, 179 (2015).

[11] C. Proust and L. Taillefer, The remarkable underlying ground states of cuprate superconductors, Annu. Rev. Condens. Matter Phys. **10**, 409 (2019).

[12] E. Bascones, B. Valenzuela, and M. Calderón, Magnetic interactions in iron superconductors: A review, C. R. Phys. **17**, 36 (2016).

[13] A. Chubukov and P. Hirschfeld, Iron-based superconductors, seven years later, Phys. Today **68**(6), 46 (2015).

[14] P. Coleman, Heavy fermions: electrons at the edge of magnetism, in *Handbook of Magnetism and Advanced Magnetic Materials*, edited by H. Kronmüller, S. Parkin, M. Fähnle, S. Maekawa, I. Zutic, J. Miltat, M. Scheinfein, G. Guntherodt, R. Wiesendanger, J. M. D. Coey, A. Inoue, and D. Awschalom (Wiley, Hoboken, NJ, 2007).

[15] Q. Si and F. Steglich, Heavy fermions and quantum phase transitions, Science **329**, 1161 (2010).

[16] F. Guinea, A. H. Castro Neto, and N. M. R. Peres, Electronic states and Landau levels in graphene stacks, Phys. Rev. B **73**, 245426 (2006).

[17] M. Koshino and E. McCann, Trigonal warping and Berry's phase $n\pi$ in ABC-stacked multilayer graphene, Phys. Rev. B **80**, 165409 (2009).

[18] F. Zhang, B. Sahu, H. Min, and A. H. MacDonald, Band structure of ABC-stacked graphene trilayers, Phys. Rev. B **82**, 035409 (2010).

[19] Y. H. Zhang and T. Senthil, Bridging Hubbard model physics and quantum Hall physics in trilayer graphene/h-BN moiré superlattice, Phys. Rev. B **99**, 205150 (2019).

[20] B. L. Chittari, G. Chen, Y. Zhang, F. Wang, and J. Jung, Gate-Tunable Topological Flat Bands in Trilayer Graphene Boron-Nitride Moiré Superlattices, Phys. Rev. Lett. **122**, 016401 (2019).

[21] P. A. Pantaleon, R. Cea, R. Brown, N. R. Walet, and F. Guinea, Narrow bands, electrostatic interactions and band topology in graphene stacks, 2D Mater. **8**, 044006 (2021).

[22] G. Chen, A. L. Sharpe, E. J. Fox, Y. H. Zhang, S. Wang, L. Jiang, B. Lyu, H. Li, K. Watanabe, T. Taniguchi, Z. Shi, T. Senthil, D. Goldhaber-Gordon, Y. Zhang, and F. Wang, Tunable correlated Chern insulator and ferromagnetism in a moiré superlattice, Nature (London) **579**, 56 (2020).

[23] H. Zhou, T. Xie, A. Ghazaryan, T. Holder, J. R. Ehrets, E. M. Spanton, T. Taniguchi, K. Watanabe, E. Berg, M. Serbyn, and A. F. Young, Half and quarter metals in rhombohedral trilayer graphene, Nature (London) **598**, 429 (2021).

[24] G. Chen, A. L. Sharpe, E. J. Fox, S. Wang, B. Lyu, L. Jiang, H. Li, K. Watanabe, T. Taniguchi, M. F. Crommie, M. A. Kastner, Z. Shi, D. Goldhaber-Gordon, Y. Zhang, and F. Wang, Tunable ferromagnetism at non-integer filling of a moiré superlattice, Nano Lett. **22**, 238 (2022).

[25] H. Zhou, T. Xie, T. Taniguchi, K. Watanabe, and A. F. Young, Superconductivity in rhombohedral trilayer graphene, Nature (London) **598**, 434 (2021).

[26] J. Yang, G. Chen, T. Han, Q. Zhang, Y.-H. Zhang, L. Jiang, B. Lyu, H. Li, K. Watanabe, T. Taniguchi, Z. Shi, T. Senthil, Y. Zhang, F. Wang, and L. Ju, Spectroscopy signatures of electron correlations in a trilayer graphene/hBN moiré superlattice, Science **375**, 1295 (2022).

[27] P. Fazekas, *Lecture Notes on Electron Correlations and Magnetism* (World Scientific, Singapore, 1999).

[28] M. Imada, A. Fujimori, and Y. Tokura, Metal-insulator transitions, Rev. Mod. Phys. **70**, 1039 (1998).

[29] D. N. Basov, R. D. Averitt, D. van der Marel, M. Dressel, and K. Haule, Electrodynamics of correlated electron materials, Rev. Mod. Phys. **83**, 471 (2011).

[30] See Supplemental Material at http://link.aps.org/supplemental/10.1103/PhysRevB.106.L081123 for further details on the model, the dynamical mean-field theory calculations, and the description of the antiferromagnetic state [19,20,31,32,34–39].

[31] A. Georges, G. Kotliar, W. Krauth, and M. J. Rozenberg, Dynamical mean-field theory of strongly correlated fermion systems and the limit of infinite dimensions, Rev. Mod. Phys. **68**, 13 (1996).

[32] G. Kotliar, S. Y. Savrasov, K. Haule, V. S. Oudovenko, O. Parcollet, and C. A. Marianetti, Electronic structure calculations with dynamical mean-field theory, Rev. Mod. Phys. **78**, 865 (2006).

[33] L. Chen, H. Hu, and Q. Si, Fragile insulator and electronic nematicity in a graphene moiré system, arXiv:2007.06086.

[34] M. J. Calderón and E. Bascones, Interactions in the 8-orbital model for twisted bilayer graphene, Phys. Rev. B **102**, 155149 (2020).

[35] M. Schüler, M. Rösner, T. O. Wehling, A. I. Lichtenstein, and M. I. Katsnelson, Optimal Hubbard Models for Materials with Nonlocal Coulomb Interactions: Graphene, Silicene, and Benzene, Phys. Rev. Lett. **111**, 036601 (2013).

[36] L. Huang, T. Ayral, S. Biermann, and P. Werner, Extended dynamical mean-field study of the Hubbard model with long-range interactions, Phys. Rev. B **90**, 195114 (2014).

[37] E. Gull, A. J. Millis, A. I. Lichtenstein, A. N. Rubtsov, M. Troyer, and P. Werner, Continuous-time Monte Carlo methods for quantum impurity models, Rev. Mod. Phys. **83**, 349 (2011).

[38] K. Haule, Quantum Monte Carlo impurity solver for cluster dynamical mean-field theory and electronic structure calculations with adjustable cluster base, Phys. Rev. B **75**, 155113 (2007).

[39] M. Jarrell and J. E. Gubernatis, Bayesian inference and the analytic continuation of imaginary-time quantum Monte Carlo data, Phys. Rep. **269**, 133 (1996).